Hindawi
Structural Control and Health Monitoring
Volume 2024, Article ID 5512085, 15 pages
https://doi.org/10.1155/2024/5512085

Research Article

Fast Force Estimation of Cable Structures Using Smartphone-Captured Video and Template Matching Algorithm

Xiao-Wei Ye,[1] **Wei-Ming Que**,[1] **Yang Ding**,[2] **and Tao Jin**[3]

[1] *Department of Civil Engineering, Zhejiang University, Hangzhou 310058, China*
[2] *Department of Civil Engineering, Hangzhou City University, Hangzhou 310015, China*
[3] *College of Civil Engineering, Zhejiang University of Technology, Hangzhou 310023, China*

Correspondence should be addressed to Yang Ding; ceyangding@zju.edu.cn

Received 27 December 2023; Revised 18 February 2024; Accepted 29 February 2024; Published 16 March 2024

Academic Editor: Xiang Shi

Cables are important components of long-span bridge structures, whose operation is significantly affected by cable force changes. Nowadays, cable force testing is performed by physical methods; that is, sensors are installed on the cable structure to monitor its force changes. Obviously, this strategy requires an extensive amount of time to achieve cable force calculation, which makes it impossible to monitor the force of the cable structure in real time. Meanwhile, smartphones have attracted extensive attention in the field of structural health monitoring (SHM) because of their higher cost-effectiveness than accelerometers, which include price and lifespan. Besides, many people own a smartphone, which leads to the possibility of a wider range of applications. Therefore, this paper presents a framework for the rapid estimation of the cable force of long-span bridges based on smartphones-captured video and a template matching algorithm. First, the empirical mode decomposition (EMD) method with wavelet decomposition (WD) method, that is, the EMDWD model, is constructed to extract the vibration signal of the bridge cable by eliminating the effects of smartphone vibration and environmental noise on the measured dynamic displacement, thus effectively improving the accuracy of data processing. In addition, the vibration identification model of bridge cable based on a template matching algorithm is established, and the deformation curve of cable is obtained. Finally, the frequency of bridge suspender is calculated by the Fourier transform method (FFT), and the cable force is estimated based on the smartphone-captured video.

1. Introduction

The cable component is an important force transmission structure of cable bridges, as the cable force affects the service life of the bridge. Therefore, it is necessary to accurately estimate the cable force [1–3]. At present, the measurement of the dynamic characteristics of cable, namely, the vibration and natural frequencies, is a paramount step for vibration-based cable force estimation [4]. Yu et al. [5] studied a wireless monitoring system for the bridge cable force based on the vibration frequency method and conducted experimental verification through laboratory and field tests. The results of field experiments showed that the relative error between the wireless monitoring system and the reference wired system was less than 0.5%. Rainieri and Fabbrocino [6] developed an original algorithm for automatic output-only modal parameter estimation and found that it was robust and could provide the accurate estimation of modal parameters including damping ratio. Therefore, this algorithm has been used to develop vibration-based tensile load estimation systems for cables and tie rods. Zarbaf et al. [7] evaluated the stay cables of the new Ironton Russell Bridge using vibration-based force estimation and compared the results with the lift-off test results. They found that the difference between the estimated force and the directly measured force (lift test) was negligible.

Obviously, to estimate the cable force, the first step is to obtain the frequency of the cable [8–11]. Nowadays, this can be performed by installing an acceleration sensor on the cable [12]. For example, Morgenthal et al. [13] proposed methods to facilitate such force recognition using a highly mobile measuring device connected to a battery-operated microcontroller and an acceleration sensor based on a modern MEMS integrated into a smartphone. The results showed that the sensor resolution and sampling rate directly influenced the accuracy of measurement and are the distinguishing criteria between competing systems. Xue and Shen [14] presented a short-time sparse time-domain algorithm combined with a simplified half-wave method. This method uses only one acceleration sensor, which makes it simple, economical, convenient, and fast. Its reliability and accuracy were verified by two experiments and one engineering application. However, this approach requires moving the sensor from one place to another to test all the cables of a large bridge, which limits its measurement efficiency [15]. In the traditional method, the accelerometer needs to be installed on the cable to obtain the cable vibration signal, which acts as the basis for estimating the cable force. However, this method has two shortcomings. On the one hand, the accelerometer needs to be installed at a certain height on the cable. Generally, this is done at a distance of more than 3 m from the bridge deck. Obviously, this necessitates a climbing operation plan that can cause traffic stop and even result in personal harm. Besides, accelerometers are expensive and have poor durability. In addition, it is not possible to install a large number of accelerometers on every bridge, as it will inevitably increase costs.

At present, computer vision has been widely used in structural health monitoring [16–20]. In recent years, the rapid development of computer vision methods has provided a new solution for the more effective estimation of cable force [21]. Kim et al. [22] constructed a vision-based monitoring system that uses image processing techniques to estimate the tension of stay cables during traffic use. Du et al. [23] used two measurement methods based on digital image technology, digital image processing, and digital image correlation to identify cable forces through the camera capture of single and multipoint images. To verify the reliability of this method, the results were compared with those obtained using an accelerometer, and the relative deviation between the two methods and the accelerometer was less than 5%. Chu et al. [24] proposed a vision-based contactless cable force monitoring system for cable frequency identification and tension estimation, and its applicability was verified through experiments. Zhang et al. [25] presented a deep learning-based complex background segmentation method to estimate the cable forces of urban bridges from UAV-collected videos. The effectiveness and robustness of this method were successfully verified by a field test of a city cable-stayed bridge.

Using a computer vision method, the vibration deformation curve of bridge cable can be obtained directly; however, because the vibration deformation curve contains a lot of environmental noise, an important step remains to evaluate the cable force, that is, data processing [26]. At present, many methods are used for this purpose, such as the wavelet decomposition (WD) method, empirical mode decomposition (EMD) method, and ensemble EMD (EEMD) [27]. For example, Swami and Jain [28] proposed an effective image denoising method that adaptively combines the features of wavelets, wave atoms, and curves. The denoised image could perfectly present the smooth area and effectively preserve the texture and edge in the image. Zhang et al. [29] used the modified EMD algorithm to denoise the fault signals prior to the maximum correlation kurtosis deconvolution. Li and Hu [30] derived a sensor fault detection method based on enhanced principal component analysis (PCA) using EEMD denoising. After EEMD preprocessing, the denoised data were smoother than the original data. Fang et al. [31] proposed an improved program based on empirical wavelet transform to eliminate the noise from Global Navigation Satellite System (GNSS) data and to identify the modal parameters of bridge structures. The above methods, however, have limitations; the accuracy of the WD method depends on the wavelet function, and the accuracy of EMD and EEMD methods depends on the number of decomposition layers, which can lead to multimodal properties of the decomposed intrinsic modal function [32]. To address these issues, Yang et al. [33] proposed a complete ensemble empirical mode decomposition with an adaptive noise joint wavelet packet threshold processing method for processing ultrasonic nondestructive testing defect signals. Compared with the EEMD algorithm, the signal-to-noise ratio was increased by 48.03%, and the root mean square error and total number of iterations were reduced by 38.77% and 33.34%, respectively.

Based on the above findings, we establish the EMDWD method for data decomposition to combine the advantages of the WD and EMD methods. This framework achieves the fast estimation of the cable force of long-span bridges based on smartphone-captured video and a template matching algorithm. Specifically, we can obtain a large number of cable vibration videos (3~5 minutes) from smartphones at the bridge sidewalk, then analyze these data and estimate the cable force. This monitoring plan will obviously not cause any traffic stops, since smartphone video recordings can be made on the sidewalk or vacant land. In addition, no climbing operations are included, thus protecting personal safety. Firstly, the EMDWD model is constructed based on the WD and EMD methods to extract the vibration signal of bridge cable. Then, the deformation curve of the cable is obtained based on the vibration identification model of the bridge cable by the template matching algorithm. Finally, the frequency of bridge cable is calculated based on FFT using smartphone-captured video, followed by the estimation of cable force.

2. Framework for Cable Force Identification

2.1. Template Matching Algorithm. Computer vision (CV) methods use digital cameras, digital sensors, smartphones, or other sensing vision devices to replace the analog vision function of the human eye [34]. Compared with traditional monitoring methods, this approach can more accurately and quantitatively identify the displacement of the structure, as shown in Figure 1. As can be seen from Figure 1, the smartphone records the global coordinates of the target point on the structure to be measured in the form of image coordinates. Changes in the image coordinates of the target point can be recorded based on fixed smartphone coordinates when the target point moves, so as to monitor the displacement and deformation of the target point [35, 36]. Meanwhile, a single camera based on the CV method cannot fully monitor the spatial displacement of structures, such as out-plane displacement. Therefore, to monitor the spatial displacement of the structure, we need at least two cameras in this method.

In order to accurately obtain the displacement and deformation curve of the structure under external force load, it is necessary to continuously monitor the structure to be tested [37, 38]. At this time, the initial deformation of the structure must be determined, that is, the initial template. With the passage of time, the structure to be tested will also vibrate and deform. Taking the initial template as the origin, the displacement curve of the structure to be tested in this period of time can be obtained [39]. At present, the gray template matching algorithm is a commonly used template matching method, which includes the average absolute difference algorithm, absolute error sum algorithm, error square sum algorithm, and square error square sum algorithm, among others [40]. In recent years, template matching algorithms have been widely applied in the field of structural health monitoring and have achieved remarkable results [11, 41, 42].

The average absolute difference algorithm calculates the sum of the absolute values of gray difference between the subimage and the template image and then averages it, as shown in equation (1). The average absolute difference is clearly smaller; hence the two graphs are rather similar [43].

$$L(i,j) = \frac{1}{M \times N} \sum_{s=1}^{M} \sum_{t=1}^{N} |P(i+s-1, j+t-1) - T(s,t)|, \tag{1}$$

where $M \times N$ denotes the size of the target graph; (i, j) denotes the pixel of the point to be measured; P is the target graph; and T is the template graph.

The absolute error sum algorithm and the average absolute difference algorithm are based on the same idea, but their similarity calculation formula is different, that is,

$$L(i,j) = \sum_{s=1}^{M} \sum_{t=1}^{N} |P(i+s-1, j+t-1) - T(s,t)|. \tag{2}$$

The error square sum algorithm is similar to the above algorithm, that is,

$$L(i,j) = \sum_{s=1}^{M} \sum_{t=1}^{N} |P(i+s-1, j+t-1) - T(s,t)|^2. \tag{3}$$

The square error square sum algorithm is similar to the above algorithm, that is,

$$L(i,j) = \frac{1}{M \times N} \sum_{s=1}^{M} \sum_{t=1}^{N} |P(i+s-1, j+t-1) - T(s,t)|^2. \tag{4}$$

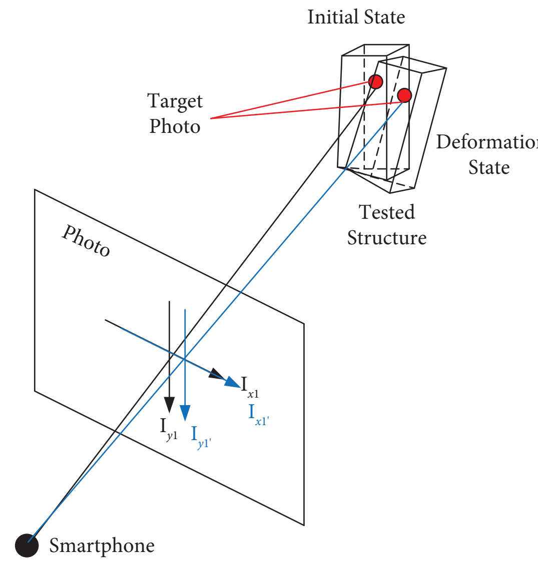

Figure 1: Computer vision method with smartphone.

2.2. Calculation of Cable Force. If the influence of cable bending stiffness, cable sag effect, and cable damper are ignored, the relationship between cable force and its natural vibration frequency can be obtained using the string vibration theory, so as to calculate the force. When the constraints at both ends of the cable structure are hinged constraints, the measurement of cable force by the frequency method can be expressed as follows [44]:

$$P = \frac{4\bar{m}L^2 f_n^2}{n^2} - \frac{n^2\pi^2 EI}{L^2}, \tag{5}$$

where f_n denotes the nth order cable frequency (Hz); P denotes the force of cable (N); E denotes the elastic modulus of cable; $\bar{m}$ denotes the mass per unit length of cable (kg/m); I denotes the moment of inertia of the cable; and L is the height of cable.

Commonly, the cable stiffness can be found in the design maps. However, the physical properties of a bridge cable can change with time, such as due to rust and corrosion on the bridge cable. Therefore, the real stiffness of the bridge cable will be lower than the design value and cannot be accurately obtained. To tackle this problem, natural frequencies of different orders are adopted to estimate the cable force, from which the specific value of cable stiffness information is no longer required. The cable force estimation formula without known stiffness is

$$P = \frac{\bar{m}L^2}{3}\left(16 f_1^2 - f_2^2\right). \tag{6}$$

The cable frequency can be calculated by the Fourier transform method (FFT), which assumes that any function can be expressed in countless series functions or integral forms, that is, the time-domain signal is converted into the frequency domain signal, and can be expressed by [45]

$$F(\omega) = F(f(t)) = \int_{-\infty}^{+\infty} f(t)e^{-i\omega t}\mathrm{d}t,$$
$$f(t) = F^{-1}(F(\omega)) = \frac{1}{2\pi}\int_{-\infty}^{+\infty} F(\omega)e^{-i\omega t}\mathrm{d}\omega, \tag{7}$$

where $f(t)$ denotes the time-domain signal; $F(\omega)$ denotes the frequency domain signal; F^{-1} denotes the inverse operation of the function; and f denotes the frequency.

3. EMDWD Method for SHM Data Reconstruction

3.1. Empirical Mode Decomposition Method. The WD method decomposes the data step by step through the wavelet function; thereby, the decomposition accuracy depends on the wavelet function. In contrast, the empirical mode decomposition (EMD) method does not need to set a function to decompose the data [46–48]. Firstly, it obtains decomposition by interpolating a certain interval data, that is, by selecting the maximum and minimum values of local data and calculating their average value. Then, it subtracts the average value from the original data to get new data. Finally, the original data is gradually decomposed into the intrinsic mode function (IMF) and residual, that is, [49].

$$P(t) = \sum_{i=1}^{n} y_i(t) + l_n(t), \tag{8}$$

where $P(t)$ represents the SHM data; $y_i(t)$ denotes the ith IMF; and $l_n(t)$ is the residual.

3.2. Wavelet Decomposition Method. Monitoring sequence data usually have waveform characteristics, and real-time sequence data have repeatability characteristics [50]. Therefore, the sequence data can be represented by "infinite" waveform functions. The wavelet decomposition (WD) method decomposes the monitoring data step by step in the way of high frequency and low frequency, that is, a time series data are decomposed by wavelet function [51]:

$$\Psi(t) = \frac{1}{\sqrt{a}}\Psi\left(\frac{t-b}{a}\right),$$
$$a = 2^j, \tag{9}$$
$$b = k2^j,$$

where t denotes the time; a represents the scale factor; b represents the translation factor; j represents the scale coefficient; and k is the translation coefficient.

By setting the threshold T for the above wavelet coefficients, the high-frequency data in the monitoring data can be filtered out; that is, the noise information contained in the wavelet function that is greater than the threshold is completely eliminated. The current approaches for the selection of threshold include the SUREShrink threshold estimation method, BayesShrink threshold estimation method, VisuShrink threshold estimation method, and Minmax threshold estimation method. For the SUREShrink threshold estimation method, the wavelet coefficients are calculated for the threshold T based on the unbiased likelihood estimation criterion, such as [52].

$$R(T) = \sum_{i=1}^{N}\left(\min\left(|y_i|, T\right)\right)^2 + \sigma_n^2 - \frac{2\sigma_n^2}{N}\sum_{i=1}^{N} I\left(|y_i| \le T\right). \tag{10}$$

For the BayesShrink threshold estimation method, the wavelet function is modeled based on statistical characteristics, and then the threshold T is obtained according to Bayesian estimation, such as [53].

$$T = \frac{\sigma_n^2}{\sigma_w}. \tag{11}$$

The VisuShrink threshold estimation method is a global threshold method. In other words, a unified threshold T is adopted for all coefficients in the wavelet function [54]:

$$T = \sigma_n\sqrt{2\ln N}. \tag{12}$$

The Minmax threshold estimation method calculates the wavelet function to obtain the threshold T based on the maximum minimization principle [55]:

$$T = \begin{cases} 0, & N \le 32, \\ 0.3936 + \dfrac{0.1829\lg N}{\lg 2}, & N \ge 32, \end{cases} \tag{13}$$

where N represents the number of wavelet function layers; σ_n represents the standard deviation of noise; σ_w represents the standard deviation of the initial wavelet function; and I denotes the judgment function.

3.3. Wavelet-Based EMD. The decomposition efficiency of the EMD method depends on the number of decomposition layers, which may cause the data confusion of decomposed eigenmodes. Therefore, this paper combines the WD and EMD methods to construct the EMDWD method. Unlike traditional EMD that extracts the signal trend by averaging the upper and lower envelopes intersecting the local maxima and minima of the signal, the wavelet-based empirical mode decomposition directly extracts the signal trend by applying the multilevel wavelet decomposition of consecutive approximations within the sifting process [56]. In specific, firstly, the EMD method is used to decompose the SHM data to obtain the IMFs and residual. Then, the IMFs and residual are processed by the WD method to obtain new IMFs and residual. Finally, the SHM data are reconstructed based on the new IMFs and residual, which can be seen in Figure 2.

4. Field Test and Cable Force Identification of a Long-Span Bridge

In this paper, the cable force identification test of a bridge cable based on computer vision was carried out for Jiubao Bridge, which is located in Hangzhou, China, and has

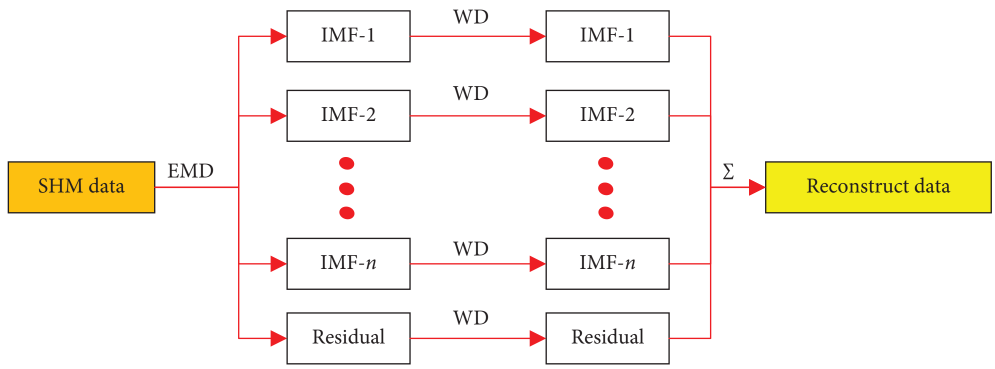

Figure 2: EMDWD method for SHM data reconstruction.

a length (main bridge) of 3 × 210 m and a total length (including the approach bridge) of 1,855 m. Firstly, we installed the low-frequency acceleration sensor (sampling frequency of 1000 Hz) at about 3~4 m height and fixed it with red tape. The installation position of the acceleration sensor is shown in Figure 3. The DH5906W accelerometer has a maximum sampling rate of 1000 Hz, its vibration acceleration is $1 \times g$, its error is less than 10%, its weight is 0.26 kg, and its size is 94 mm × 56 mm × 26 mm. This type of accelerometer can be applied with the following restrictions: (1) the stiffness of the cable should not be too large and (2) the slenderness ratio of the cable cannot be less than 10. This test took the longest Cable C1 in the left span cable system as the standard reference, and tested the longest Cable C2, Cable C3, and shortest Cable C4 in the middle span boom system of Jiubao Bridge.

The acceleration signals of the four cables (C1, C2, C3, and C4) of the measured bridge are shown in Figures 4(a)–7(a), respectively. The acceleration signal was further converted in combination with the FFT method to calculate the first-order and second-order frequencies of the four cables, as shown in Figures 4(b)–7(b), respectively. The first peak in the frequency spectra represents the frequency of the accelerometer, which is a sensor with zero fundamental frequency.

Next, the smartphone was fixed in the direction perpendicular to the bridge cable. Finally, the pixel coordinate change of the target point was calculated according to the video data and combined with the template matching algorithm. The frequency of the cable was calculated based on the FFT, and then the cable force was estimated. The test arrangement is shown in Figure 8. As can be seen from the figure, the layout orientation of the smartphone is perpendicular to the vibration direction of the cable, which is convenient for capturing the motion law of the cable. The smartphone was placed at a horizontal distance of 2 m from the cable and a perpendicular distance of less than 1 m from the red tape. The diameter of the cable was 0.077 m.

Generally, we used the accelerometer to measure the vibration frequency of the cable over a period of few seconds, because the sampling frequency of the accelerometer is higher than that of cable vibration. Meanwhile, we needed more time to capture videos of cable vibrations when using smartphones. In addition, more video data is required to effectively eliminate the impact of environmental and mobile phone vibrations. To compensate for these, the video frame rate was low. The red tape is obviously different from the color of background and environment; hence, it was taken as the target point in the video. We adopted Mate30 smartphone with TAS-AL00 model as the vision equipment, in which the video resolution is 16 : 9, 1080 p, and the video frame rate is 30 fps, that is, a one-second video is composed of 30 images, and the screen is 2340 × 1080. The size of the template is 400 ∗ 300 pixels. The monitoring video image and template image are shown in Figure 9. The raw video will be directly computed without undergoing any further processing. We arranged the acceleration sensor along the direction of the cable. During the monitoring process, we tried to keep the posture of the smartphone parallel to the cable as much as possible to ensure that the smartphone image coordinates are parallel to the direction of the accelerometer.

According to the video data recorded on the bridge deck, a gray template matching model based on the square error square sum algorithm was established to obtain the vibration curve of the cable. It is important to note that smartphones are vulnerable to environmental loads during shooting, resulting in mobile phone vibration, which will lead to the original vibration ($S_y(t)$) measured by the video data, including the real vibration of cable ($S_t(t)$), environmental vibration ($S_h(t)$), and smartphone vibration ($S_s(t)$), which can be expressed as

$$S_y(t) = S_t(t) + S_h(t) + S_s(t). \tag{14}$$

Smartphone vibration is always present and fixed. According to the literature, the vibration frequency of smartphones is very low. Environmental vibration is related to the surrounding wind field, vehicles, pedestrians, etc., which leads to its significant uncertainty. To address the above challenges, firstly, we obtained the measured acceleration data of the standard cable and converted it into deformation data. Then, we used smartphones to obtain deformation data of the cable under multisource loads. Finally, we determined the sum of smartphone vibration data and environmental vibration data by subtracting the measured data based on smartphone deformation data. Both types of vibration vary over time and are not constant values.

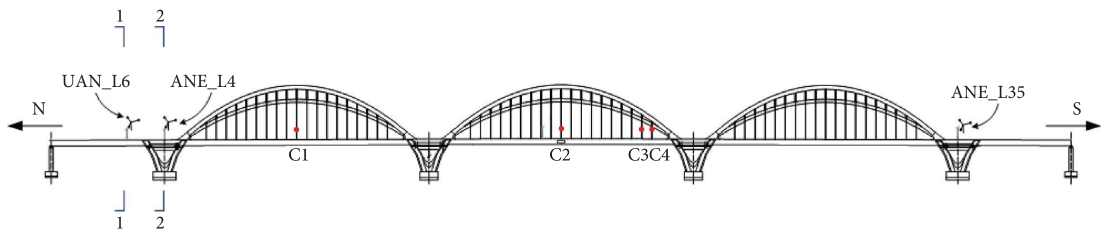

Figure 3: Installation position of acceleration sensor.

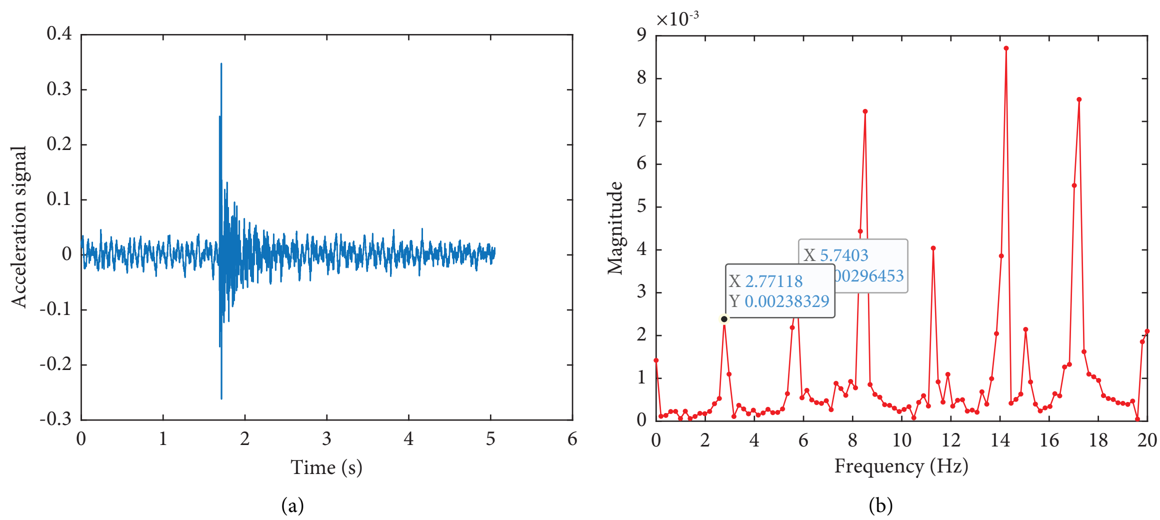

Figure 4: Frequency of Cable C1 with acceleration sensor. (a) Acceleration signal of Cable C1. (b) Calculation frequency of Cable C1.

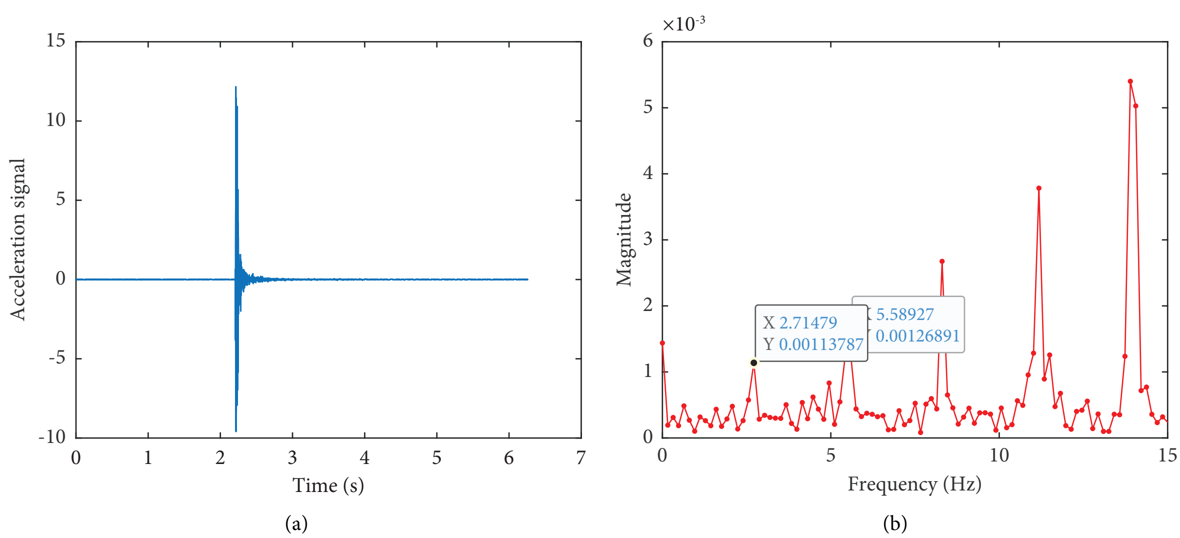

Figure 5: Frequency of Cable C2 with acceleration sensor. (a) Acceleration signal of Cable C2. (b) Calculation frequency of Cable C2.

However, considering that we only have four cables to capture in our recording and the relatively short time required to obtain their vibration video data; we assumed that the environmental vibration would not change within 5 minutes. We immediately conducted visual monitoring of other cable vibrations using smartphones to obtain deformation data of the cables under multisource loads. Also, we obtained the sum of smartphone vibration data and environmental vibration data. As a result, we could calculate the actual vibration data of the cable. It should be noted that the vibration deformation data of the same vibration captured from different shooting angles exhibit certain differences. This represents intuitive time-domain information. However, the frequency information extracted in this paper

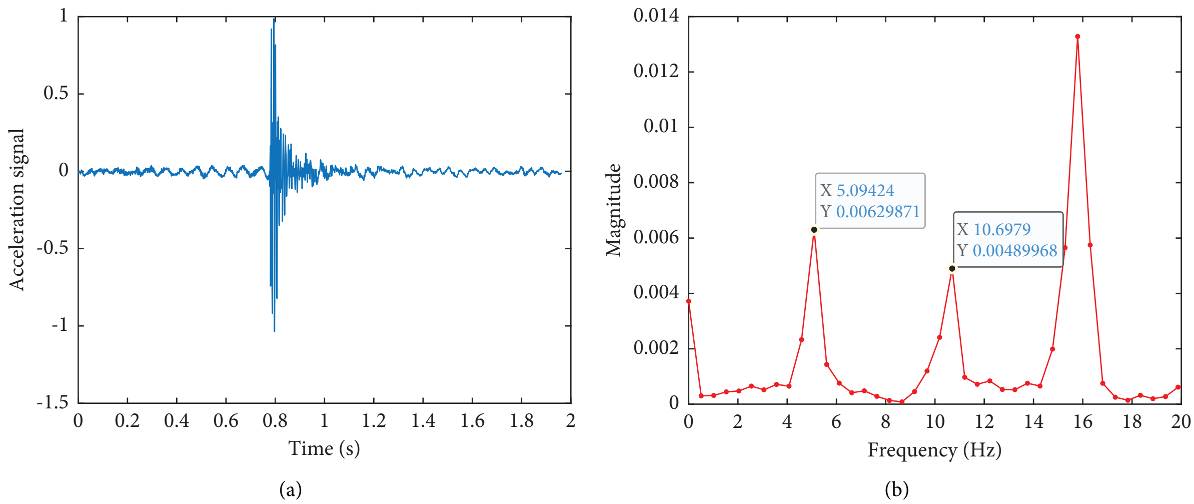

Figure 6: Frequency of Cable C3 with acceleration sensor. (a) Acceleration signal of Cable C3. (b) Calculation frequency of Cable C3.

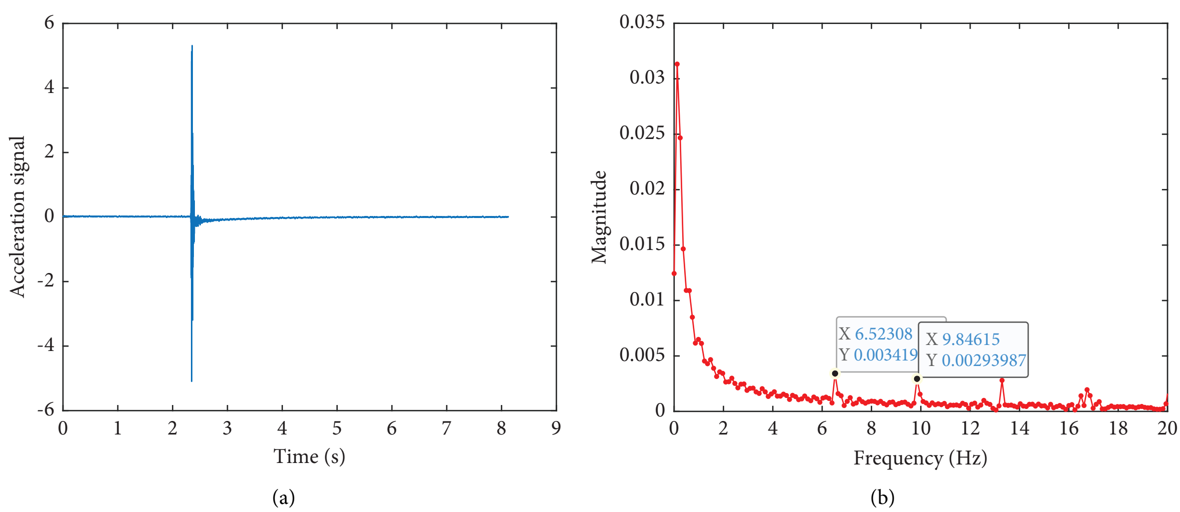

Figure 7: Frequency of Cable C4 with acceleration sensor. (a) Acceleration signal of Cable C4. (b) Calculation frequency of Cable C4.

Figure 8: Visual monitoring of bridge cable.

Figure 9: Monitoring of cable using smartphone. (a) Video image. (b) Template image.

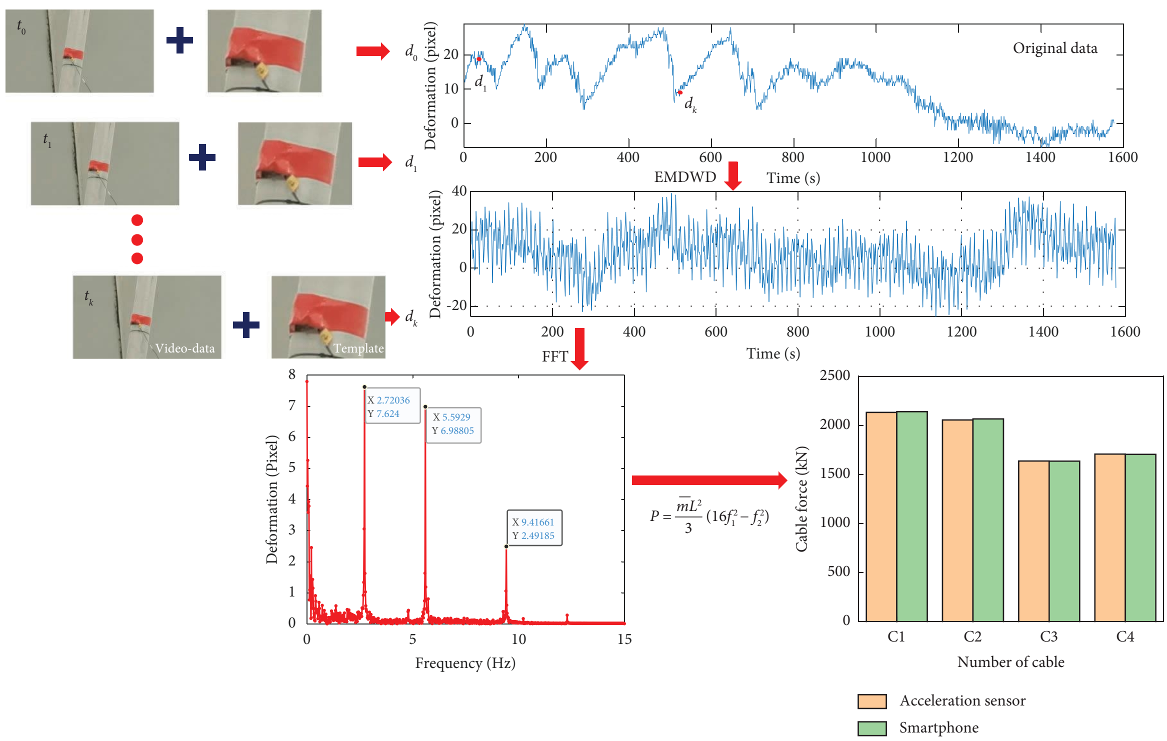

Figure 10: Flowchart of cable force measurement based on CV using smartphone.

is obtained through data processing and is minimally affected by variations in the captured videos. By doing this, we can ensure the same results of the same vibration data in different locations and at different resolutions, so this technology can be used in the video images shot by different mobile phones.

For example, we took C1 cable as the standard cable, that is, subtracting the video data ($S_y(t)$) from the measured data ($S_t(t)$) to obtain the basic ambient noise value at first. Then, the noise reduction data were decomposed and reconstructed according to the EMDWD method. Finally, the frequency of signal data were calculated by the FFT method, and the flowchart is shown in Figure 10.

The SHM data processing and calculation results are shown in Figures 11–14. At first, we obtained the frequency value of C1 according to the accelerometer signal of C1. Then, we generated a set of smartphone signals based on C1 frequency values, which we assume were the real vibration signals of C1 cable ($S_t(t)$). Finally, we used the measured smartphone signal to subtract real vibration signals, and thus we can acquired the environmental vibration ($S_h(t)$) and mobile phone vibration signal data ($S_s(t)$). To accomplish this task, we used a smartphone to take a video of four cables vibrating simultaneously. Therefore, we assumed that the measurement noise of each cable during this period was the same.

Furthermore, we conducted control experiments based on Cable C2 signals to analyze the impact of EMD, WD, WDEMD, and EMDWD methods on signal data processing, which can be seen in Figure 12. We used traditional EMD and WD methods to process the Cable C2 data. This entails using the WD method to denoise data at first, then using the EMD method to decompose the signal, to finally reconstruct the signal. As can be seen Figure 12, when we used the WD

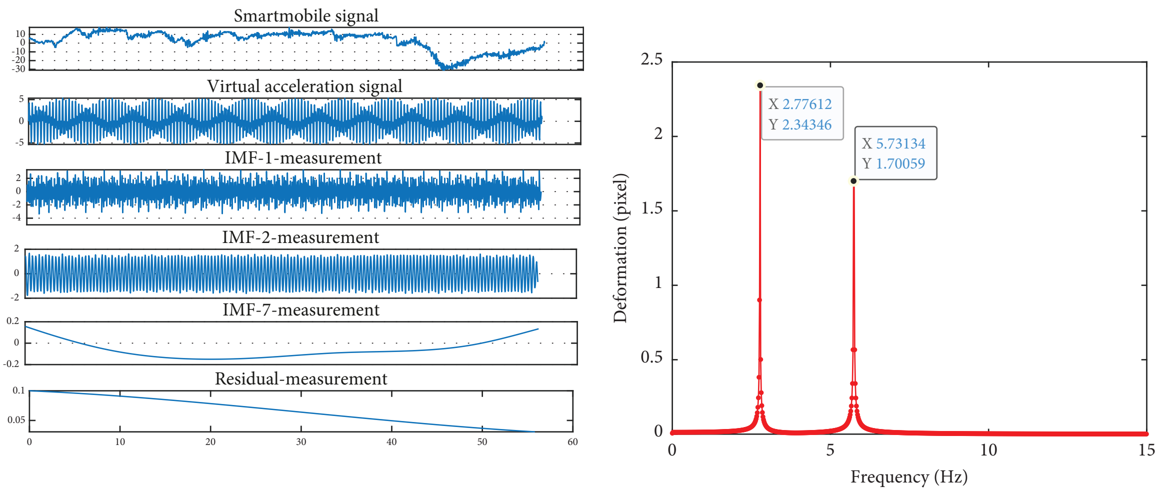

(a) (b)

Figure 11: Frequency of Cable C1 by CV using smartphone. (a) Data processing of Cable C1 by EMDWD. (b) Calculation frequency of Cable C1.

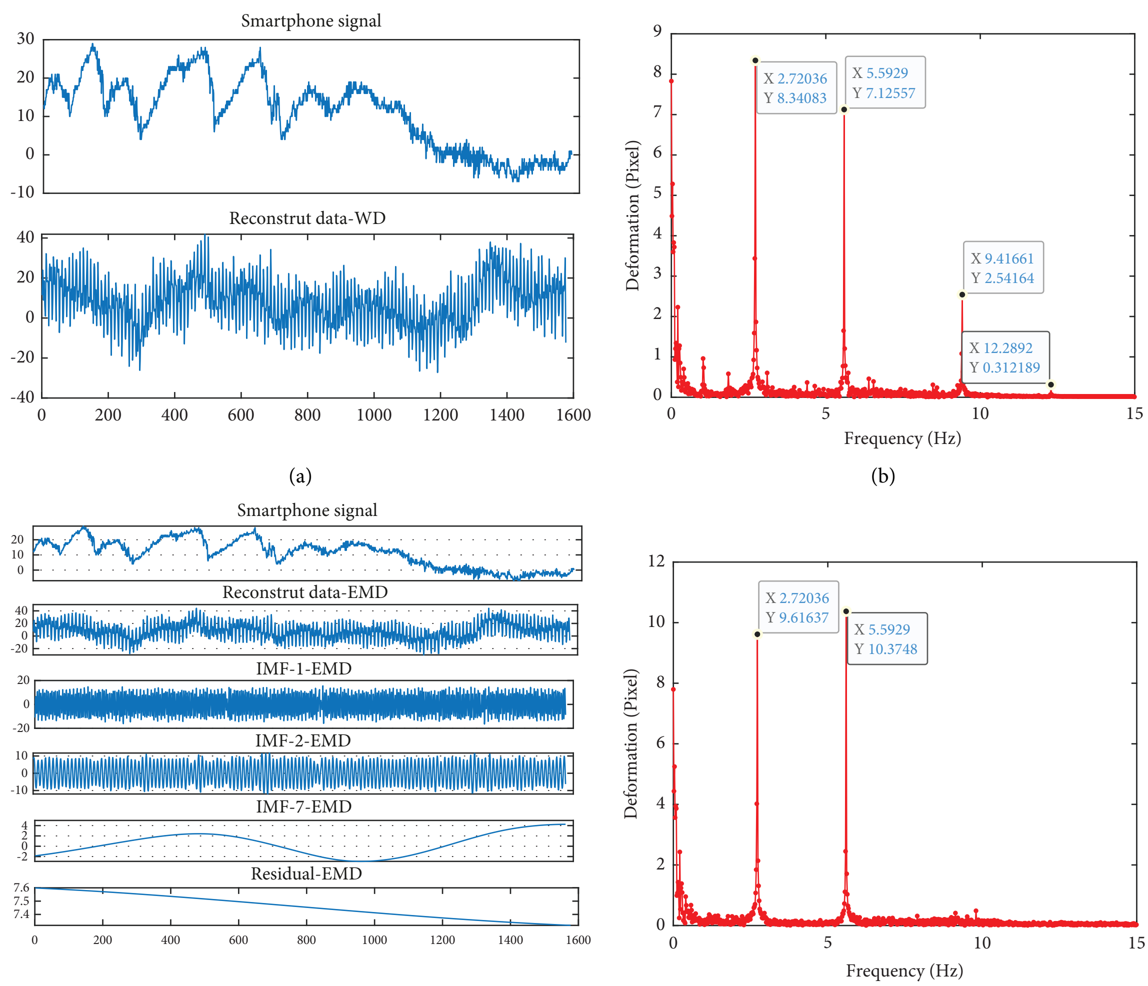

(c) (d)

Figure 12: Continued.

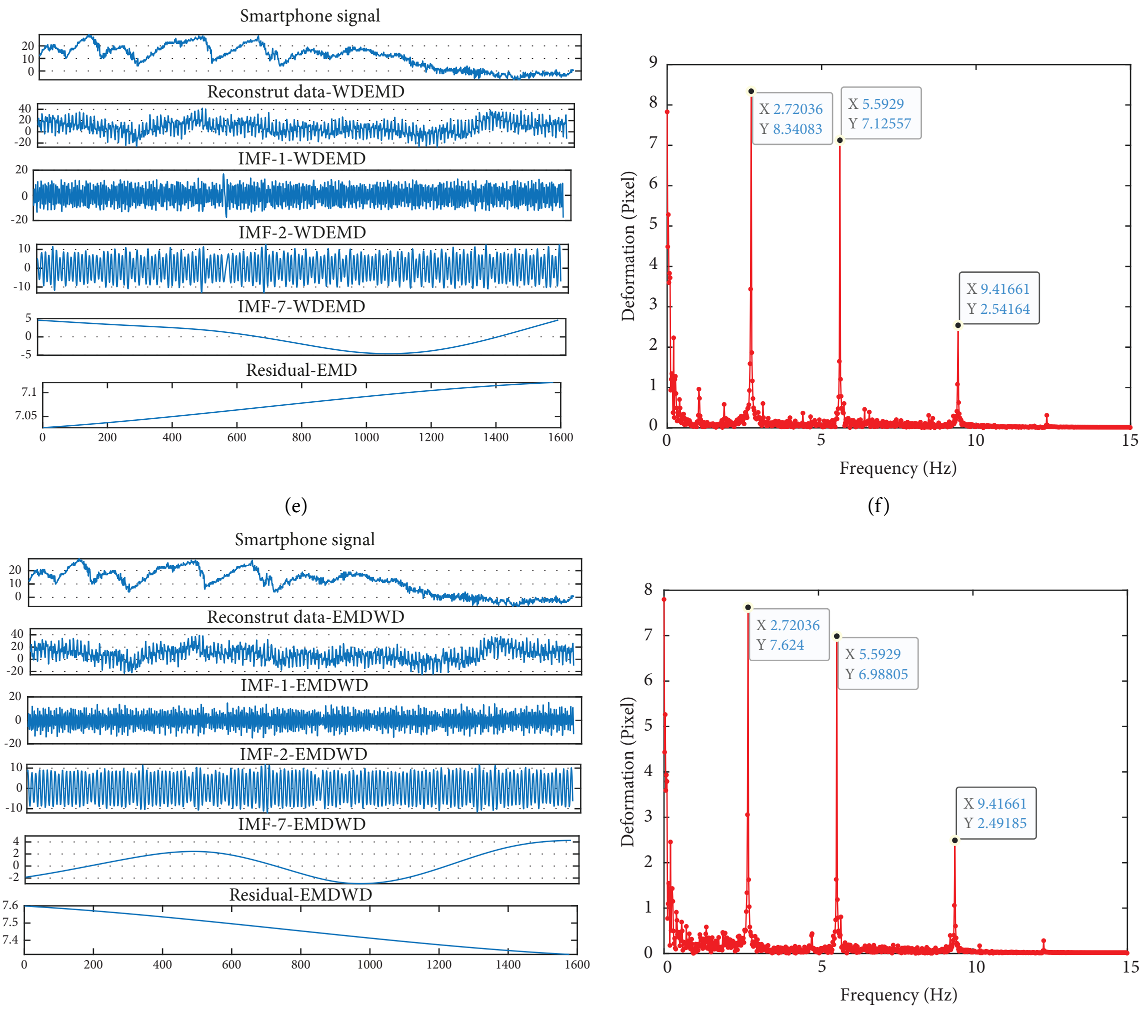

(e) (f)

(g) (h)

FIGURE 12: Frequency of Cable C2 by CV with smartphone. (a) Data processing of Cable C2 by WD. (b) Calculation frequency of Cable C2 by WD. (c) Data processing of Cable C2 by EMD. (d) Calculation frequency of Cable C2 by EMD. (e) Data processing of Cable C2 by WDEMD. (f) Calculation frequency of Cable C2 by WDEMD. (g) Data processing of Cable C2 by EMDWD. (h) Calculation frequency of Cable C2 by EMDWD.

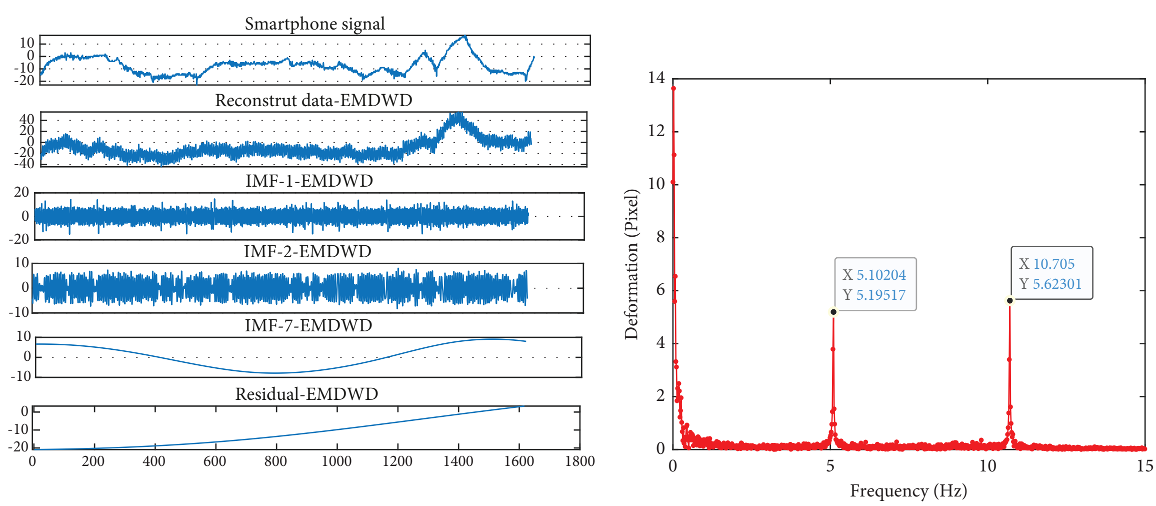

(a) (b)

FIGURE 13: Frequency of Cable C3 by CV using smartphone. (a) Data processing of Cable C3 by EMDWD. (b) Calculation frequency of Cable C3.

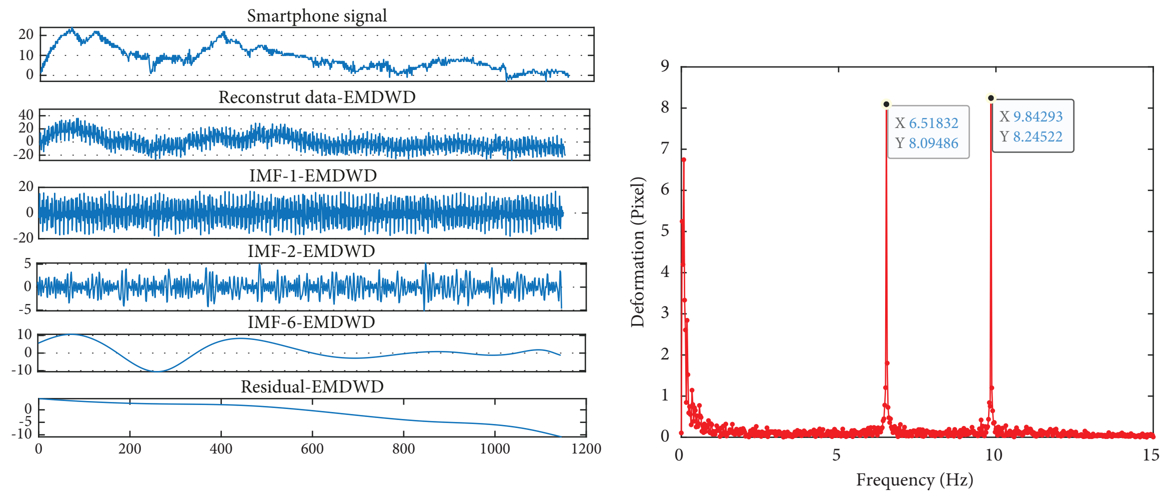

(a) (b)

Figure 14: Frequency of Cable C4 by CV using smartphone. (a) Data processing of Cable C4 by EMDWD. (b) Calculation frequency of Cable C4.

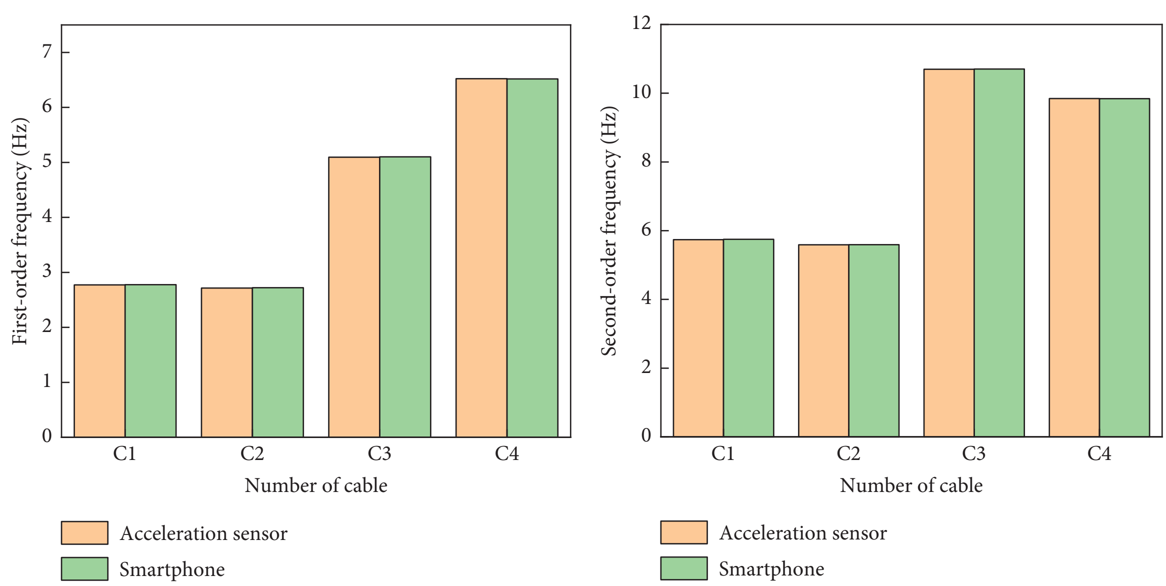

(a) (b)

Figure 15: Continued.

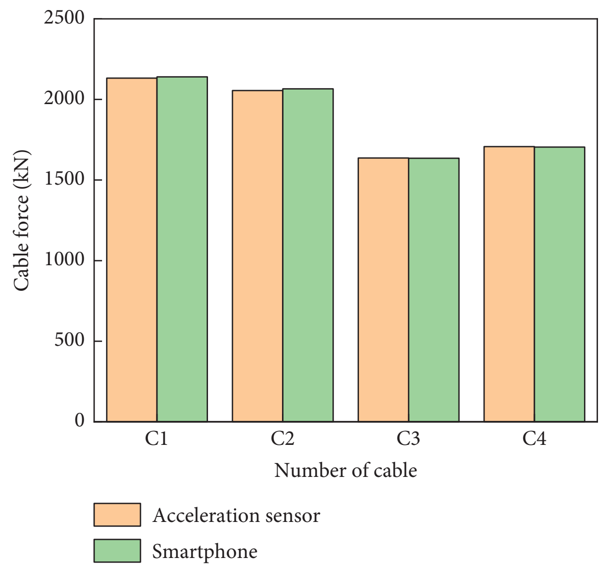

(c)

Figure 15: Comparison of results between acceleration sensor and smartphone. (a) Comparison of first-order frequency. (b) Comparison of second-order frequency. (c) Comparison of cable force.

Table 1: Error of cable force.

Cable number	C1	C2	C3	C4
Acceleration sensor (kN)	2132.4	2055.6	1636.8	1707.4
Smartphone (kN)	2140.3	2066.1	1635.3	1704.6
Error (%)	0.37	0.51	0.09	0.16

method, there was signal interference between 0 and 2 Hz, i.e., data noise, which makes it difficult to accurately determine the first-order frequency of the cable. On the contrary, the EMD method can effectively denoise signals from 0 to 2 Hz, so that we can obtain smoother curves. However, the EMD method cannot effectively capture higher-order frequencies, i.e., the third-order frequency of the cable, while the WD method can mine more effective information in the signal. Therefore, it was necessary to combine the two above methods to fully reflect the effective information of data. The EMDWD method could effectively denoise signals of 0~2 Hz compared to the WDEMD, which demonstrates its efficacy in combining the advantages of EMD and WD methods. In other words, the EMDWD method used in this article is more effective.

Next, we used the EMDWD method to calculate the frequency of Cable C3 and Cable C4. It can be seen that the EMDWD method could effectively capture the cable frequency and provide data support for subsequent cable force evaluation.

For Cable C1 and C2, the mass per unit length was about 44.68 kg/m and the length was about 39.9 m; for Cable C3, the mass per unit length was about 59.25 kg/m and the length was about 16.6 m; for Cable C4, the mass per unit length was about 44.75 kg/m and the length was about 14.0 m. The diameter of all cables was about 0.077 m. We brought these cable parameters into equation (12) and compared the estimated cable force, as shown in Figure 15. It can be seen from the figure that the calculated frequency and force of cable based on computer vision is in good agreement with the measured frequency and force. Table 1 presents the discrepancies in cable force as determined through visual measurements versus actual measurements. It can be observed that the cable force measured visually exhibits relatively minor deviations when compared to the actual values, indicating a certain degree of reliability.

5. Conclusions

Smartphones have a higher cost-effectiveness than accelerometers, which includes price and lifespan. In addition, most people have a smartphone, which allows for a wider range of applications. Although the measurement accuracy of accelerometers is better than smartphones, the latter are a more economical alternative if the aim is not to monitor displacement but to perform the estimation of cable force. Therefore, this paper presents a framework for estimating the cable force of long-span bridges based on smartphone-captured video and deep learning. Firstly, the EMDWD model was constructed based on the WD and EMD methods, which could effectively improve the accuracy of data processing. Then, the vibration identification model of bridge cable based on a template matching algorithm was established, and the deformation curve of the cable was obtained. Finally, based on smartphone-captured videos, the frequency of bridge suspender was calculated and the cable force was estimated. Several conclusions can be drawn from the results: (1) By setting obvious mark points and based on the template matching algorithm, the vibration curve of bridge cable can be obtained effectively. (2) The proposed the EMDWD method can decompose the measured displacement into cable vibration and environmental vibration. By reconstructing the noise reduction data, the cable vibration signal can be effectively extracted. (3) The effectiveness and robustness of the proposed framework were verified by the field test of the long-span bridge. The results indicate that the cable forces estimated by using the proposed method are almost the same as the measured values.

In this paper, in addition to the influence of environmental vibration on video data, for the template matching algorithm, video picture background noise will also affect the test data, so how to accurately extract the goal of the cable is an important problem. In the following research, we will consider using multiple video images to estimate the spatial displacement of the cable and semantic segmentation to more effectively eliminate the background noise. Since the template matching requires the manual selection of the template for the tracking calculation, which is limited by the selection of the template, the quality of the template can affect the estimation results of the cable force. Therefore, we will consider a variety of algorithms in the future, based on the computer automatically extract cable features for deformation calculation.

Data Availability

The data used to support the findings of the study are available from the corresponding author upon request.

Conflicts of Interest

The authors declare that they have no conflicts of interest.

Authors' Contributions

Xiao-Wei Ye and Yang Ding designed the research. Yang Ding processed the corresponding data. Yang Ding wrote the first draft of the manuscript. Wei-Ming Que and Tao Jin helped to organize the manuscript. Xiao-Wei Ye and Yang Ding revised and edited the final version.

Acknowledgments

The authors would like to acknowledge the support provided by the National Key R&D Program of China (Grant no. 2022YFC3802301), the National Science Foundation of China (Grant no. 52178306), the Ministry of Education of Humanities and Social Science Project (No. 23YJCZH037), the Educational Science Planning Project of Zhejiang Province (No. 2023SCG222), the Foundation of the State Key Laboratory of Mountain Bridge and Tunnel Engineering (No. SKLBT-2210), and the Scientific Research Project of Zhejiang Provincial Department of Education (No. Y202248682).

References

[1] Y. Ding, X. W. Ye, H. Zhang, and X. S. Zhang, "Fatigue life evolution of steel wire considering corrosion-fatigue coupling effect: analytical model and application," *Steel and Composite Structures*, vol. 50, no. 3, pp. 363–374, 2024.

[2] Y. Ding, X. W. Ye, Y. H. Su, and X. L. Zheng, "A framework of cable wire failure mode deduction based on Bayesian network," *Structures*, vol. 57, no. 11, Article ID 104996, 2023.

[3] S. W. Kim, D. U. Park, J. S. Kim, and J. B. Park, "Estimating tension of a prestressed concrete cable-stayed bridge under construction and traffic use conditions using a vision-based system," *Structures*, vol. 47, pp. 299–312, 2023.

[4] S. Kangas, A. Helmicki, V. Hunt, R. Sexton, and J. Swanson, "Cable-stayed bridges: case study for ambient vibration-based cable tension estimation," *Journal of Bridge Engineering*, vol. 17, no. 6, pp. 839–846, 2012.

[5] Y. Yu, C. Zhang, X. Zhu, W. H. Kang, X. Mao, and B. Uy, "Design and experimental investigations of a vibration based wireless measurement system for bridge cable tension monitoring," *Advances in Structural Engineering*, vol. 17, no. 11, pp. 1657–1668, 2014.

[6] C. Rainieri and G. Fabbrocino, "Development and validation of an automated operational modal analysis algorithm for vibration-based monitoring and tensile load estimation," *Mechanical Systems and Signal Processing*, vol. 60-61, pp. 512–534, 2015.

[7] S. E. H. A. M. Zarbaf, M. Norouzi, R. J. Allemang, V. J. Hunt, A. Helmicki, and C. Venkatesh, "Ironton-russell bridge: application of vibration-based cable tension estimation," *Journal of Structural Engineering*, vol. 144, no. 6, Article ID 04018066, 2018.

[8] Y. Ding, X. W. Ye, and Y. Guo, "A multistep direct and indirect strategy for predicting wind direction based on the EMD-LSTM model," *Structural Control and Health Monitoring*, vol. 2023, Article ID 4950487, 13 pages, 2023.

[9] W. Wang, D. Cui, C. Ai et al., "Target-free recognition of cable vibration in complex backgrounds based on computer vision," *Mechanical Systems and Signal Processing*, vol. 197, Article ID 110392, 2023.

[10] S. Yu, J. Zhang, Z. Su, and P. Jiang, "Fast and robust vision-based cable force monitoring method free from environmental disturbances," *Mechanical Systems and Signal Processing*, vol. 201, Article ID 110617, 2023.

[11] D. Feng and M. Q. Feng, "Computer vision for SHM of civil infrastructure: from dynamic response measurement to damage detection–A review," *Engineering Structures*, vol. 156, pp. 105–117, 2018.

[12] H. P. Wan, L. Su, D. M. Frangopol, Z. Chang, W. X. Ren, and X. Ling, "Seismic response of a bridge crossing a canyon to near-fault acceleration-pulse ground motions," *Journal of Bridge Engineering*, vol. 26, no. 6, Article ID 05021006, 2021.

[13] G. Morgenthal, S. Rau, J. Taraben, and T. Abbas, "Determination of stay-cable forces using highly mobile vibration measurement devices," *Journal of Bridge Engineering*, vol. 23, no. 2, Article ID 04017136, 2018.

[14] S. Xue and R. Shen, "Real time cable force identification by short time sparse time domain algorithm with half wave," *Measurement*, vol. 152, Article ID 107355, 2020.

[15] D. Feng, T. Scarangello, M. Q. Feng, and Q. Ye, "Cable tension force estimate using novel noncontact vision-based sensor," *Measurement*, vol. 99, pp. 44–52, 2017.

[16] G. Jeon, S. Kim, S. Ahn, H. Kim, and H. Yoon, "Vision-based automatic cable displacement measurement using Cable-ROI Net and Uni-KLT," *Structural Control and Health Monitoring*, vol. 29, no. 8, Article ID e2977, 2022.

[17] W. Du, D. Lei, F. Zhu, P. Bai, and J. Zhang, "A non-contact displacement measurement system based on a portable smartphone with digital image methods," *Structure and Infrastructure Engineering*, vol. 2022, Article ID 2141268, 19 pages, 2022.

[18] D. Jana, S. Nagarajaiah, and Y. Yang, "Computer vision-based real-time cable tension estimation algorithm using complexity pursuit from video and its application in Fred-Hartman cable-stayed bridge," *Structural Control and Health Monitoring*, vol. 29, no. 9, Article ID e2985, 2022.

[19] H. Sarmadi, A. Entezami, K. V. Yuen, and B. Behkamal, "Review on smartphone sensing technology for structural health monitoring," *Measurement*, vol. 223, Article ID 113716, 2023.

[20] Y. Zhang and K. V. Yuen, "Time-frequency fusion features-based incremental network for smartphone measured structural seismic response classification," *Engineering Structures*, vol. 278, Article ID 115575, 2023.

[21] Y. Tian, C. Zhang, S. Jiang, J. Zhang, and W. Duan, "Non-contact cable force estimation with unmanned aerial vehicle and computer vision," *Computer-Aided Civil and Infrastructure Engineering*, vol. 36, no. 1, pp. 73–88, 2021.

[22] S. W. Kim, B. G. Jeon, N. S. Kim, and J. C. Park, "Vision-based monitoring system for evaluating cable tensile forces on a cable-stayed bridge," *Structural Health Monitoring*, vol. 12, no. 5-6, pp. 440–456, 2013.

[23] W. Du, D. Lei, P. Bai, F. Zhu, and Z. Huang, "Dynamic measurement of stay-cable force using digital image techniques," *Measurement*, vol. 151, Article ID 107211, 2020.

[24] C. Chu, F. Ghrib, and S. Cheng, "Cable tension monitoring through feature-based video image processing," *Journal of Civil Structural Health Monitoring*, vol. 11, no. 1, pp. 69–84, 2021.

[25] C. Zhang, Y. Tian, and J. Zhang, "Complex image background segmentation for cable force estimation of urban bridges with drone-captured video and deep learning," *Structural Control and Health Monitoring*, vol. 29, no. 4, 2021.

[26] L. Sun, Y. Li, and W. Zhang, "Experimental study on continuous bridge-deflection estimation through inclination and strain," *Journal of Bridge Engineering*, vol. 25, no. 5, Article ID 04020020, 2020.

[27] J. Zheng, J. Cheng, and Y. Yang, "Partly ensemble empirical mode decomposition: an improved noise-assisted method for eliminating mode mixing," *Signal Processing*, vol. 96, pp. 362–374, 2014.

[28] P. D. Swami and A. Jain, "Image denoising by supervised adaptive fusion of decomposed images restored using wave atom, curvelet and wavelet transform," *Signal, Image and Video Processing*, vol. 8, no. 3, pp. 443–459, 2014.

[29] X. Zhang, J. Kang, L. Hao, L. Cai, and J. Zhao, "Bearing fault diagnosis and degradation analysis based on improved empirical mode decomposition and maximum correlated kurtosis deconvolution," *Journal of Vibroengineering*, vol. 17, no. 1, pp. 243–260, 2015.

[30] G. Li and Y. Hu, "An enhanced PCA-based chiller sensor fault detection method using ensemble empirical mode decomposition based denoising," *Energy and Buildings*, vol. 183, pp. 311–324, 2019.

[31] Z. Fang, J. Yu, and X. Meng, "Modal parameters identification of bridge structures from GNSS data using the improved empirical wavelet transform," *Remote Sensing*, vol. 13, no. 17, p. 3375, 2021.

[32] S. Huang, X. Wang, C. Li, and C. Kang, "Data decomposition method combining permutation entropy and spectral substitution with ensemble empirical mode decomposition," *Measurement*, vol. 139, pp. 438–453, 2019.

[33] Y. Yang, S. Li, C. Li, H. He, and Q. Zhang, "Research on ultrasonic signal processing algorithm based on CEEMDAN joint wavelet packet thresholding," *Measurement*, vol. 201, Article ID 111751, 2022.

[34] N. Metni and T. Hamel, "A UAV for bridge inspection: visual servoing control law with orientation limits," *Automation in Construction*, vol. 17, no. 1, pp. 3–10, 2007.

[35] Y. Xu, J. M. W. Brownjohn, D. Hester, and K. Y. Koo, "Long-span bridges: enhanced data fusion of GPS displacement and deck accelerations," *Engineering Structures*, vol. 147, pp. 639–651, 2017.

[36] S. Chen, D. F. Laefer, E. Mangina, S. M. I. Zolanvari, and J. Byrne, "UAV bridge inspection through evaluated 3D reconstructions," *Journal of Bridge Engineering*, vol. 24, no. 4, Article ID 05019001, 2019.

[37] M. Gindy, R. Vaccaro, H. Nassif, and J. Velde, "A state-space approach for deriving bridge displacement from acceleration," *Computer-Aided Civil and Infrastructure Engineering*, vol. 23, no. 4, pp. 281–290, 2008.

[38] R. J. Greenbaum, A. W. Smyth, and M. N. Chatzis, "Monocular computer vision method for the experimental study of three-dimensional rocking motion," *Journal of Engineering Mechanics*, vol. 142, no. 1, Article ID 04015062, 2016.

[39] S. Yu, Z. Xu, Z. Su, and J. Zhang, "Two flexible vision-based methods for remote deflection monitoring of a long-span bridge," *Measurement*, vol. 181, Article ID 109658, 2021.

[40] L. Deng, W. Yan, and S. Li, "Computer modeling and weight limit analysis for bridge structure fatigue using opensees," *Journal of Bridge Engineering*, vol. 24, no. 8, Article ID 04019081, 2019.

[41] W. Du, D. Lei, Z. Hang, Y. Ling, P. Bai, and F. Zhu, "Short-distance and long-distance bridge displacement measurement based on template matching and feature detection methods," *Journal of Civil Structural Health Monitoring*, vol. 13, no. 2-3, pp. 343–360, 2023.

[42] P. Xiao, Z. Y. Wu, R. Christenson, and S. Lobo-Aguilar, "Development of video analytics with template matching methods for using camera as sensor and application to highway bridge structural health monitoring," *Journal of Civil Structural Health Monitoring*, vol. 10, no. 3, pp. 405–424, 2020.

[43] H. Li, J. Ou, X. Zhao et al., "Structural health monitoring system for the Shandong Binzhou Yellow River highway bridge," *Computer-Aided Civil and Infrastructure Engineering*, vol. 21, no. 4, pp. 306–317, 2006.

[44] L. Wang, X. Zhang, S. Huang, and L. Li, "Measured frequency for the estimation of cable force by vibration method," *Journal of Engineering Mechanics*, vol. 141, no. 2, Article ID 06014020, 2015.

[45] Y. C. Ni, M. M. Alamdari, X. W. Ye, and F. L. Zhang, "Fast operational modal analysis of a single-tower cable-stayed bridge by a bayesian method," *Measurement*, vol. 174, no. 12, Article ID 109048, 2021.

[46] C. Z. Dong and F. N. Catbas, “A review of computer vision–based structural health monitoring at local and global levels,” *Structural Health Monitoring*, vol. 20, no. 2, pp. 692–743, 2021.

[47] S. Jeong, H. Kim, J. Lee, and S. H. Sim, “Automated wireless monitoring system for cable tension forces using deep learning,” *Structural Health Monitoring*, vol. 20, no. 4, pp. 1805–1821, 2021.

[48] S. Yu, J. Zhang, and X. He, “An advanced vision-based deformation measurement method and application on a long--span cable-stayed bridge,” *Measurement Science and Technology*, vol. 31, no. 6, Article ID 065201, 2020.

[49] N. Qiao, L. H. Wang, Q. Y. Liu, and H. Q. Zhai, “Multi-scale eigenvalues Empirical Mode Decomposition for geomagnetic signal filtering,” *Measurement*, vol. 146, pp. 885–891, 2019.

[50] W. Sandham, D. Hamilton, A. Fisher, W. Xu, and M. Conway, “Multiresolution wavelet decomposition of the seismocardiogram,” *IEEE Transactions on Signal Processing*, vol. 46, no. 9, pp. 2541–2543, 1998.

[51] M. Wang and M. Van Der Schaar, “Operational rate-distortion modeling for wavelet video coders,” *IEEE Transactions on Signal Processing*, vol. 54, no. 9, pp. 3505–3517, 2006.

[52] D. Benaouda, F. Murtagh, J. L. Starck, and O. Renaud, “Wavelet-based nonlinear multiscale decomposition model for electricity load forecasting,” *Neurocomputing*, vol. 70, no. 1-3, pp. 139–154, 2006.

[53] M. Hashemi and S. Beheshti, “Adaptive noise variance estimation in BayesShrink,” *IEEE Signal Processing Letters*, vol. 17, no. 1, pp. 12–15, 2010.

[54] M. Bekara, L. Knockaert, A. K. Seghouane, and G. Fleury, “A model selection approach to signal denoising using Kullback’s symmetric divergence,” *Signal Processing*, vol. 86, no. 7, pp. 1400–1409, 2006.

[55] F. M. Janeiro and P. M. Ramos, “Threshold estimation for least-squares fitting in impedance spectroscopy,” *Measurement*, vol. 124, pp. 479–485, 2018.

[56] S. A. Bagherzadeh and M. Salehi, “Analysis of in-flight cabin vibration of a turboprop airplane by proposing a novel noise-tolerant signal decomposition method,” *Journal of Vibration and Control*, vol. 28, no. 17-18, pp. 2226–2239, 2021.